

The Relation between Structure and Corrosion Protection Performance of Hybrid Nanonanosilica/Sol-Gel Film

Yadong Fan, Yongjie Cao, Junxi Zhang*

Shanghai Key Laboratory of Material Protection and Advanced Material in Electric Power, Shanghai University of Electric Power, Shanghai, 200090, China

*E-mail: zhangjunxi@shiep.edu.cn

Received: 6 March 2019 / Accepted: 1 May 2019 / Published: 10 June 2019

The purpose of this work is to study the effect of nanofibrous SiO₂ on the corrosion protection performance of the sol-gel film coated on AA5052 aluminum alloy. The structure and surface morphology of the hybrid film were evaluated by Transmission electron microscope (TEM) and Scanning electron microscopy (SEM), the result highlighted that the surface of composite films appears uniform and the nanofibrous SiO₂ was evenly dispersed in the film. By analyzing the results of infrared spectroscopy, the addition of nanofibrous SiO₂ enhanced the cross-linking of the sol-gel film. The electrochemical behavior of coated samples was determined by electrochemical test. The corrosion protection performance of the sol-gel film had a great improvement with addition of nanofibrous SiO₂, the optimal additive concentration was 1 mg/ml at which the hybrid film showed the best corrosion protective performance in 3.5% NaCl solution. From the result of potentiodynamic polarization, the corrosion rate of sample coated with the sol-gel film with 1 mg/ml nanofibrous SiO₂ was about 6 times slower than pure sol-gel film coated sample.

Keywords: nanofibrous SiO₂; TEOS film; corrosion protective properties; electrochemistry

1. INTRODUCTION

The application of aluminum alloys widely exists in the various industry for its' excellent physical and chemical properties. However, aluminum alloys are particularly susceptible to pitting corrosion in environments containing aggressive chloride. With the increasing demand for environmentally friendly coatings, tradition chromate conversion coating has been recognized to be replaced duo to its toxicity and carcinogenic.[1] Under the comprehensive consideration, inorganic coating has been considered as a substitute for its' excellent corrosion protection performance and environmentally friendly.[2-4]But pure inorganic sol-gel film have many defects that limits its use. For

example, it's difficult to form a thicker coating without cracking for brittleness of inorganic coatings, which leads to pure sol-gel film is always difficult to possess excellent corrosion protection performance.[5]

In order to make inorganic sol-gel film widely available, a great number of works have done to improve the defect of the inorganic sol-gel film.[6-10] For instance, common additives for ameliorating the shortcoming of sol-gel coating include functional polymers, corrosion inhibitors and barrier pigments and so on.[11-13] S. Ono et al. synthesized a polyvinyl butyral (PVB) and SiO_2 hybrid coating coated on aluminum alloy substrate, the corrosion protection performance of the coating was assessed through salt spray testing, and result showed that coating contained SiO_2 -1 wt% PVB possessed best corrosion protection performance.[14] A ZrO_2 -PMMA (polymethylmethacrylate) hybrid film also coated on aluminum alloy substrate and the film containing 17 vol.% PMMA had the best corrosion protection properties. the hybrid coating still kept excellent corrosion protection even after long time immersion, which may duo to formation of stable covalent bonds between the nanoparticle and matrix that enhanced cross-linking density of the sol-gel film.[15] Beside, adding of corrosion inhibitors is another way to enhance the protective properties of sol-gel film. For example, $\text{Ce}(\text{CH}_3\text{COO})_3$ as an efficient corrosion inhibitor not only eased corrosion process of for their self-healing ability, but also CH_3COO^- could enhance hydrolysis and deposition of the sol-gel film.[16] Introduction of organic mixtures or organic corrosion inhibitors could effectively solve some of the disadvantages of inorganic coatings. However, the introduced organic additives may degrade the coating properties due to ultraviolet degradation during the coating service.

Inorganic additives as excellent filler have caught lots of research's sight for its good properties, which can be divided into 3D nanoparticles and 2D nanosheets even more some 1D nano-additive.[17] May et al. reported that epoxy/sol-gel system had excellent thermal stability with addition of 3D Al_2O_3 nanoparticles.[18] Meanwhile, embedding the two-dimensional additives in coating enhanced barrier property of the coating, two-dimensional additives restrained permeation of moisture corrosive ion extended and tortuous diffusion path.[19] Such as, Yu et al[20] confirmed that GO can effective improve barrier properties obtained film on aluminum alloy for its two dimensional structure. Also, electrospinning nanofibers were added to sol-gel coating, the result shows that the hybrid coating still keep good corrosion resistance of the aluminum even after longer exposure times.[21] However, challenges such as the dispersion of the additives and integrity of the coating still present in sol-gel film preparation.

According to the previous study, it was found that nano-clay process superb distribution in the sol-gel matrix.[22] Therefore, it is expected that using nanofibrous SiO_2 as 1D additive just like adding straw to the mud to improve the performance of sol-gel coating. The nano-scale chrysotile asbestos is obtained by opening and dispersing the chrysotile asbestos fiber bundle, and the nanofibrous silica (nanofibrous SiO_2) with excellent performance is prepared by using chrysotile asbestos as a template. The method has the advantages of simple process and low cost, which realizes the sustainable development of enterprises and mineral resources. Asbestos is harmful to people's health, but chrysotile asbestos is harmless and available. Chrysotile asbestos has been explored for it excellent properties in preparation of high specific surface silica and microlithography. [23, 24]

In this work, the chrysotile asbestos was emulsified and dispersed by sodium dodecyl benzene sulfonate (SDBS) as a surface dispersing agent, and then the fully dispersed fibrillated asbestos fiber was subjected to acid leaching to obtain pure amorphous nanofibrous SiO₂. Tetraethoxysilane (TEOS) as a precursor was used to synthesize a sol solution. Subsequently, the nanofibrous SiO₂ effect of sol-gel film on the corrosion of AA5052 aluminium alloy was investigated in 3.5 wt% NaCl solution. Hybrid sol-gel film was obtained through dipping way. AA5052 samples were dipped into the sol solution containing selected nanofibrous SiO₂ concentration. The effect of nanofibrous SiO₂ concentration on the morphology and structure of the coatings was observed by SEM, TEM. The results showed that the addition of nanofibrous SiO₂ reduced the brittleness of the coating and formed a crack free coating. At the same time, the results of FTIR spectroscopy confirmed that the cross-linking of the sol-gel films was also enhanced. The incorporation of nanofibrous SiO₂ improved the corrosion protection performance of sol-gel film by analyzing electrochemical data.

2. EXPERIMENTAL

2.1. Substrate preparation

AA5052 aluminum alloy samples (approximate minority components: Si, 0.25wt%; Cu, 0.10wt%; Mg, 2.20~2.80wt%; Zn, 0.10wt%; Mn, 0.10wt%; Cr, 0.15~0.35wt%; Fe, 0.40wt%; balance Al) (30×12×3 mm) were used, the samples were ground using diamond waterproof sandpaper to 2000 grit. And then samples were cleaned in acetone (10 min) and methanol (5 min) by using ultrasonic wave (SCQ-250A). Samples were dried with warm air after cleaned with deionized water.

2.2 Preparation Nanofibrous Silica

10 g chrysotile asbestos was added in 100 mL deionized water at room temperature. Under vigorous stirring, 1.5 g SDBS was added. After stirring for 30 minutes, the sample was kept at room temperature for 24 hours. Subsequently, the sample was thoroughly dispersed using an emulsifier machine (MBE-10L-E type emulsifier machine, Shanghai Xinrui Electrical Co., Ltd) at 6000 r/min for 1 h. To remove the residual ions, the sample was cleaned 3 times with deionized water after filtration. Then, the sample was added to 100ml of 40% sulfuric acid. After stirring for 20 minutes, the mixture was then placed in a 100 °C chamber for 4 h. After cooling, filtering and washing repeatedly until its pH value is neutral. The cleaned filter residue is dried and ground to obtain the final sample.

2.3 Preparation hybrid sol-gel films

The sol suspension was synthesized by 10 ml tetraethoxysilane (TEOS) and 20 mL ethanol and 10 mL deionized water, then pH of the suspension was adjusted to 3.5 with acetic acid in beaker. The suspension was stirred continuously for 2 h to make sure mixed fully and kept for 48 h at 25°C for complete hydrolysis. Different amounts nanofibrous SiO₂ were added to the sol to obtain 0.5, 1 and 2

mg/mL suspension respectively. The sol-gel films were prepared by immersing bare substrate in sol solution for 2min then withdrawn at 5cm/min. The coated samples were heat-treated at 60 °C for 80 min, 90°C for 40 min and 150°C for 10 min in oven. The samples were labeled as SiO₂-0 film, SiO₂-0.5 film, SiO₂-1 film and SiO₂-2 film, which correspond to the concentration of nanofibrous SiO₂ in sol.

2.4 Characterization

The surface morphology of the sol-gel coating was studied through SEM (JSM-7800F, JEOL, Tokyo, Japan). and the crystallographic information of the as-prepared samples was studied through X-ray diffraction (D8 Advance powder, Bruker ,Germany), using a Cu K α radiation X-ray diffractometer ($\lambda = 0.1546$ nm), and the scanning speed 2θ ranged from 5° to 80° was 1° min⁻¹. The structure of the sol-gel film with concentrate at 1 mg/mL was obtained by high-resolution transmission electron microscopy (HR-TEM, JEM-2100F, Japan). 2000 mesh copper grid was immersed in a sol to obtain a composite sol-gel film sample for observation by TEM. The chemical structure of the coating was analyzed by Fourier Transform infrared spectroscopy (FTIR, Agilent Cary 660). The electrochemical measurements (electrochemical impedance spectroscopy, polarization curve measurements) were tested on electrochemical workstation (Reference 1000, Gamry, USA) in 3.5% NaCl solution. Polarization curve measurements were carried out with sweeping the potential from -0.1 V to 0.1 V (vs. open-circuit potential) with a scan rate of 0.1667 mV / s. The corrosion current density of polarization curves was fitted by the fitting tool (nonlinear fitting in a weakly polarized region) provided by the Gamry 1000 electrochemical workstation. EIS measurements were conducted on the sample at open circuit potential with a 5 mV sinusoidal perturbation in the frequency range from 10⁵ Hz to 0.01 Hz after 1 h, 72 h, 168 h immersion time. EIS data were analyzed by Zview software. The samples were kept in the 3.5% NaCl solution for 1 h prior to the electrochemical tests. All the potentials were with respect to saturated calomel electrode (SCE). All tests were tested at room temperature.

3. RESULTS AND DISCUSSION

3.1 Chemical composition of nanofibrous SiO₂

X-ray (XRD) powder patterns collected for pure chrysotile asbestos and after acid pickling chrysotile asbestos are shown in Fig. 1a and b. All the diffraction peaks of chrysotile asbestos are in a good agreement with the standard PDF card (JCPDS No.25-0645) and additional peaks are observed for impurity brucite and conformed from PDF card (JCPDS No.07-0239). The main ingredient in the sample is chrysotile, which also contains a certain amount of brucite impurities. After the optimum acid leaching process (as shown in Fig. 1b), the chrysotile asbestos had completely transformed into amorphous SiO₂, and other impurity brucite were acid-etched and washed away. Fig. 2a shows SEM image of one fiber bundle in the original asbestos, which consist of many fine chrysotile asbestos. The

diameter of the fiber bundle is about 2 μm and the fibers are tightly bonded. The typical SEM image shows the presence of nanofibrous SiO_2 shape as single nanofibrous columnar with length at 200 nm to 1 μm and diameter at 50 nm. As shown in Fig. 2b, this indicates that the tubular structure of the chrysotile asbestos did not collapse due to acid leaching and dispersed very well. The length and diameter of the pickled sample are smaller than the pure sample. The morphology of the nanofibrous SiO_2 is relatively straight and the surface is smooth. And small amount of nanofibrous SiO_2 had been slightly agglomerated due to the electrostatic force between the fibers.

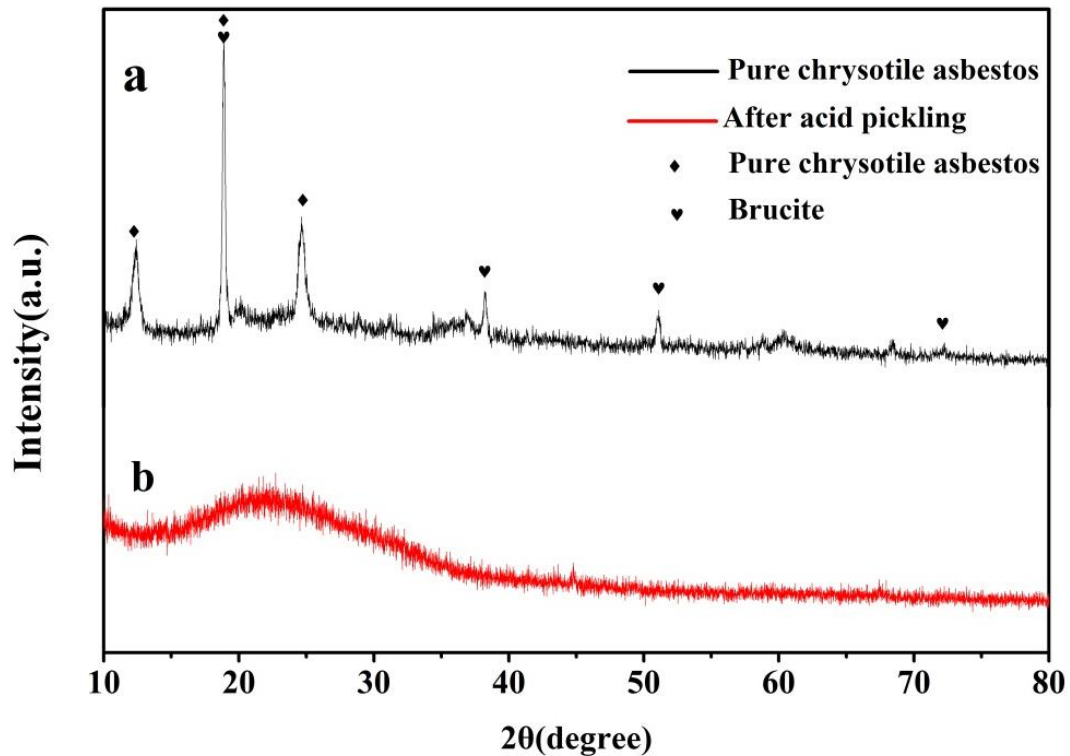


Figure 1. XRD patterns of (a) pure chrysotile asbestos (b) after acid pickling chrysotile asbestos

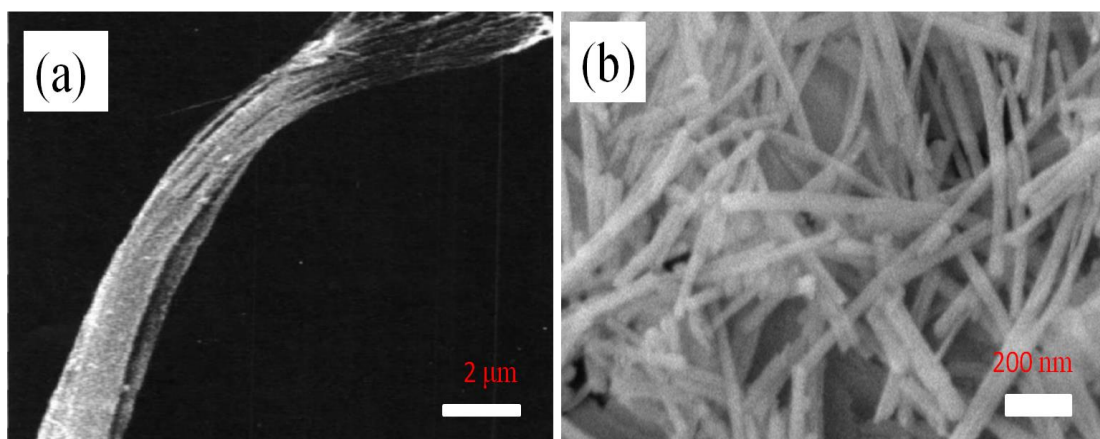


Figure 2. SEM images of nanofibrous asbestos and synthetic nanofibrous SiO_2 .

3.2 SEM image of surface topography of sol-gel/ nanofibrous SiO₂ films at different concentrate

The surface topography hybrid sol-gel film at selection concentrations is show in Fig. 3. Fig. 3a present the surface of pure sol-gel film had multiple cracks. However, surface defects of hybrid films have been greatly eliminated with incorporation of nanofibrous SiO₂, local uplifts can be observed on the surface of nanofibrous SiO₂ -0.5 and 1 film (Fig. 3b and c). Simultaneously, it is clear to observe the distribution of nanofibrous SiO₂ from the surface of sol-gel film. Agglomeration of nanofibrous SiO₂ can be observed on the surface of nanofibrous SiO₂-2 film (Fig. 3d). micropores caused by the excess addition of nanofibrous SiO₂ also can be observed clearly, this may result in a reduction in the corrosion protection performance of the sol-gel film.

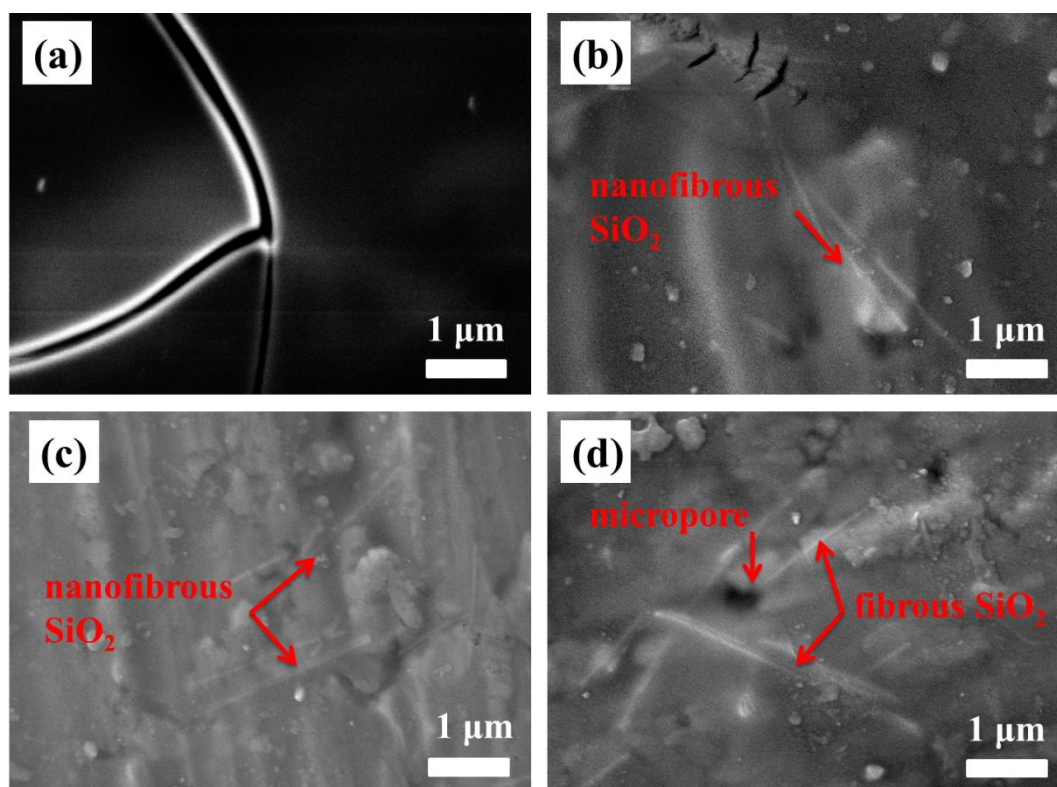


Figure 3. SEM surface topography of pure sol-gel film and hybrid sol-gel films at selection concentrations (b) SiO₂-0.5 film (c) SiO₂-1 film (d) SiO₂-2 film

3.3 SEM image of cross-section surface of sol-gel/ nanofibrous SiO₂ films

The thickness of the SiO₂ -1 film is about 9.1 μm as observed by the cross-sectional SEM presented in Fig. 4a. Fig. 4b presents the cross-sectional image of sol-gel film at higher magnification shows the presence of nanofibrous SiO₂ in the sol-gel film. Meanwhile, nanofibrous SiO₂ arranged in different directions can be observed, which illustrate that nanofibrous SiO₂ is disorderly arranged in the coating. Fig.4c shows the TEM image of SiO₂-1 film. Nanofibrous SiO₂ with different length evenly dispersed in the sol-gel film.

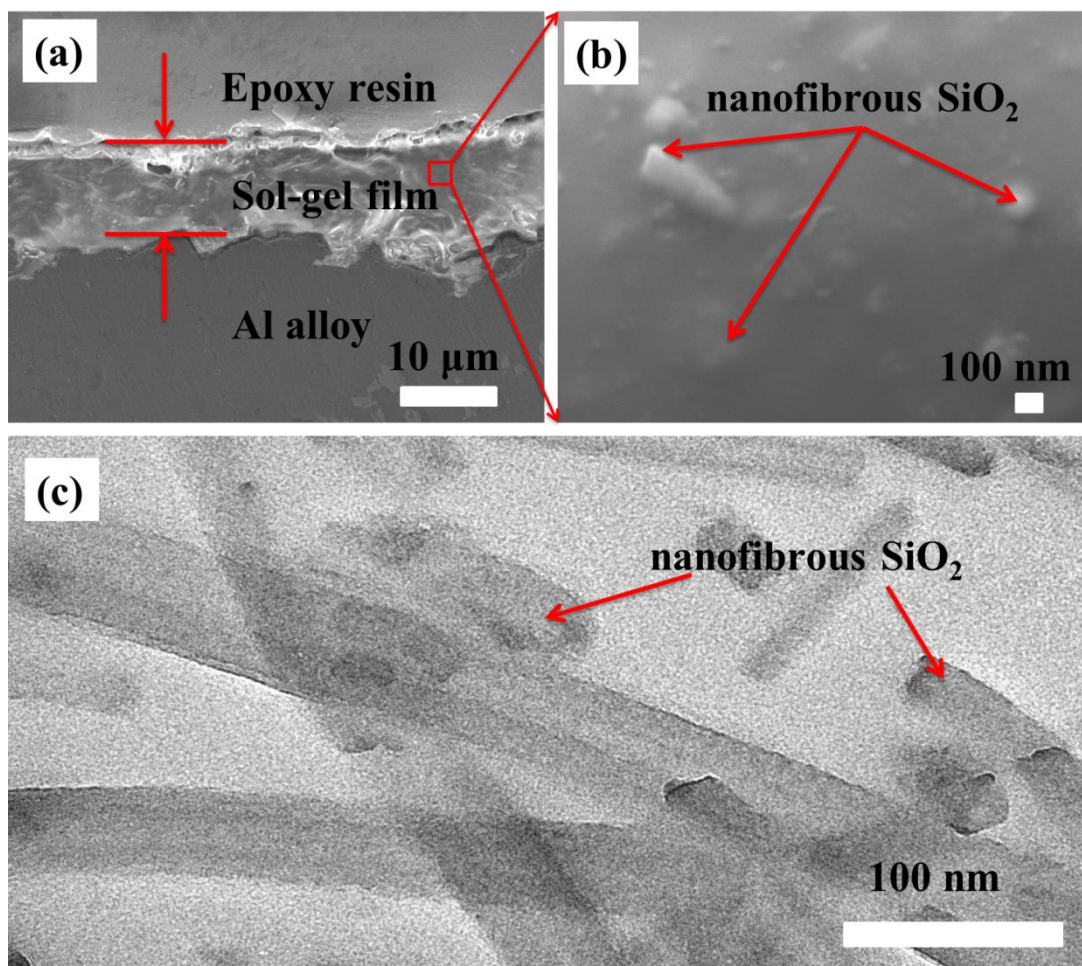


Figure 4. SEM images of cross sections of (a) SiO₂-1 coated sample. (b) high multiple SEM of cross sections SiO₂-1 coated sample (c)TEM image of SiO₂-1 film

3.4 FTIR spectra of the sol-gel/ nanofibrous SiO₂ film and nanofibrous SiO₂

Fig. 5 presents the FTIR spectra of the sol-gel/nanofibrous SiO₂ film and nanofibrous SiO₂. The band at $\sim 1080\text{ cm}^{-1}$ is assigned to the stretching vibrations of $\sim\text{Si-O}$. The band at 950 cm^{-1} are observed, which corresponds to the Si-OH vibration. The bands at ~ 800 and $\sim 460\text{ cm}^{-1}$ are related to Si-O-Si bending vibrations.[25] The increase in intensity of the bending vibrations at ~ 800 and $\sim 460\text{ cm}^{-1}$ can be related to cross-linking reactions of the sol-gel film, which indicate that the incorporation of nanofibrous SiO₂ enhance the cross-linking reaction of silanol groups, becoming more dense structure of sol/gel films[20]. A broad peak in $3000\text{--}3700\text{ cm}^{-1}$, associated mainly with O-H stretching vibration decrease with an increase in the concentration of additive nanofibrous SiO₂. The coating with fewer O-H groups is developed form the additive nanofibrous SiO₂ with higher concentration. The fewer surface O-H groups coating contains, the more dense coating is,[26] which indicate that the addition of nanofibrous SiO₂ enhance the cross-linking of the sol-gel film.

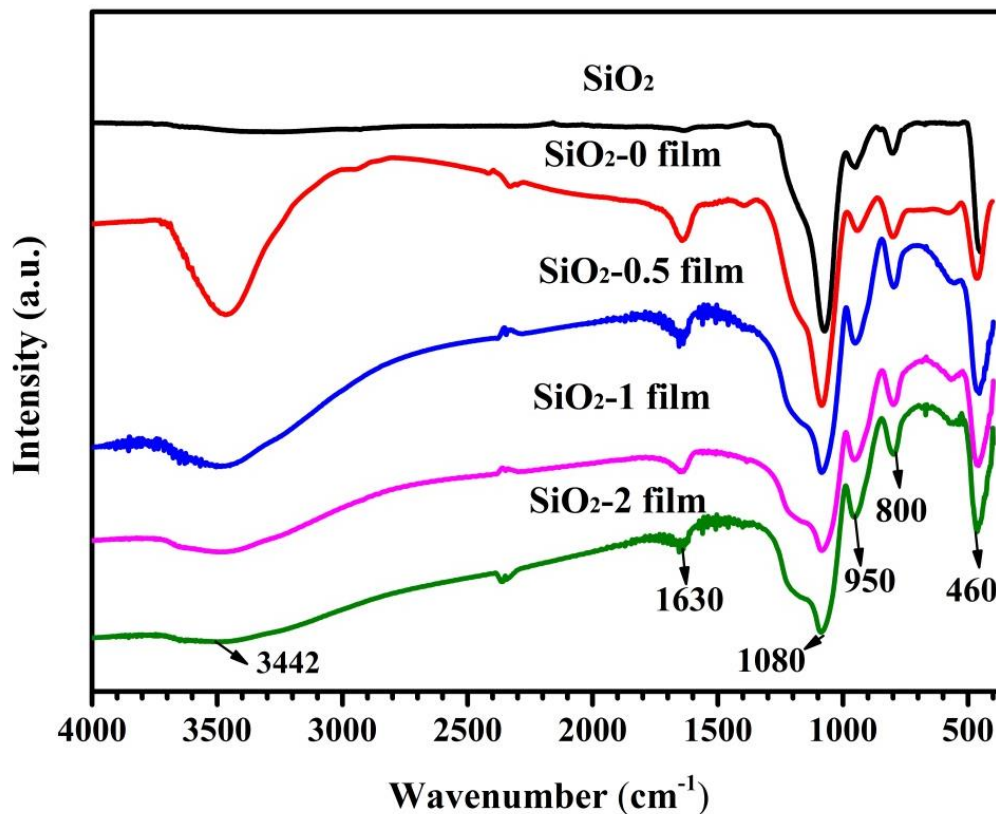


Figure 5. FTIR spectra of sol-gel/nanofibrous SiO₂ film at various nanofibrous SiO₂ concentration

3.5 Electrochemical test of sol-gel films

The potentiodynamic polarization curves for bare Al-alloy sample and sol-gel/nanofibrous SiO₂ coated samples are showed in the Fig.6. **Table 1** presents the results of the Tafel extrapolation and derived parameters of the polarization curves. The addition of nanofibrous SiO₂ has great influence on both anodic and cathodic responses. Anodic Tafel slopes (b_a) value of sol-gel/nanofibrous SiO₂ is smaller than the bare Al-alloy sample and pure sol-gel sample. The result illustrate anodic dissolution process ($\text{Al} \rightarrow \text{Al}^{3+} + 3e$) was weakened for the sol-gel/nanofibrous SiO₂ films.[27-28] The cathodic Tafel slopes ($-b_c$) decrease with increasing content of nanofibrous SiO₂. Simultaneously, the cathodic density decrease with adding of nanofibrous SiO₂, the result showed the enhanced cross-linking density of the sol-gel film inhibits the process of dissolved oxygen ($\text{O}_2 + 2\text{H}_2\text{O} + 4e \rightarrow 4\text{OH}^-$) reaching the interface of the substrate/film.[29-30] Thereby the corrosion process of the substrate is prevented. Overall, the value of corrosion current density (I_{corr}) of samples revealed that the corrosion protection performance of sol-gel film depends on the amounts of embedded nanofibrous SiO₂. With the increasing of nanofibrous SiO₂ amounts, the value of corrosion current density gradually decrease from 0.294 to 0.0581 $\mu\text{A}\cdot\text{cm}^{-2}$. While adding excessive amounts of nanofibrous SiO₂ (2 mg/ mL), the value of corrosion current density increased to 0.103 $\mu\text{A}\cdot\text{cm}^{-2}$. The addition of nanofibrous SiO₂ not only guarantees the integrity of the coating, at the same time, nanofibrous SiO₂ also can enhance cross-linking density. The penetration of aggressive ions and dissolved oxygen in the solution to the

coating/substrate interface is more suppressed by the more dense coating. On the other hand, the increase of current density of SiO₂-2 film coated sample is due to formation of the micropores on the sol-gel film integrity caused by embedding excessive nanofibrous SiO₂.

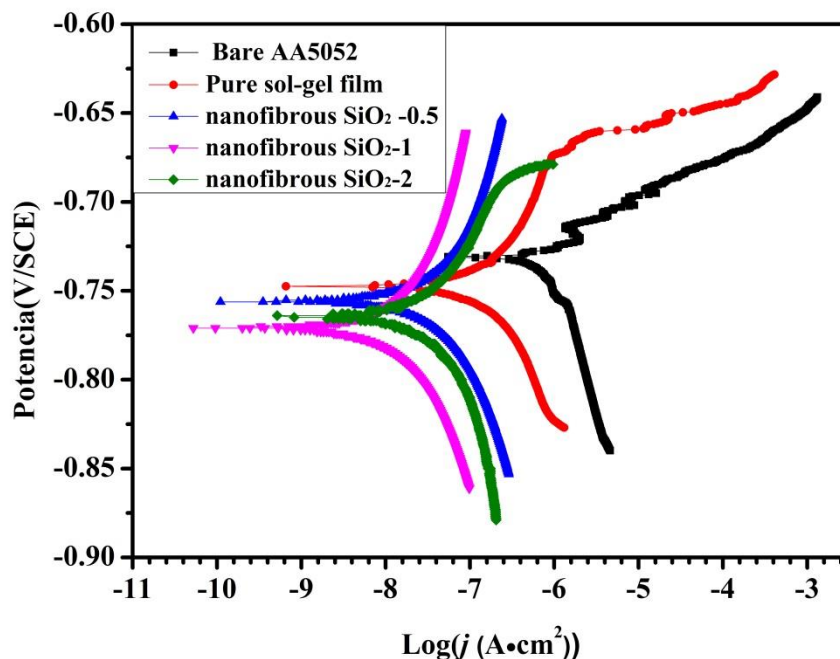


Figure 6. Potentiodynamic polarization curves of bare alloy sample and samples coated with sol-gel film modified by different amount nanofibrous SiO₂ in 3.5% NaCl solution for 1 h immersion.

Table 1. Polarization curve-derived parameters of bare Al sample and samples coated with sol-gel film modified by different amount nanofibrous SiO₂

Coating	E_{corr} (V/SCE)	j_{corr} ($\mu\text{A}\cdot\text{cm}^{-2}$)	ba($\text{V}\cdot\text{dec}^{-1}$)	-bc($\text{V}\cdot\text{dec}^{-1}$)
Bare AA5052	-0.731	0.824	0.015	0.128
Pure sol-gel film	-0.749	0.294	0.051	0.062
Nanofibrous SiO ₂ -0.5	-0.755	0.193	0.352	0.364
Nanofibrous SiO ₂ -1	-0.764	0.058	0.358	0.541
Nanofibrous SiO ₂ -2	0.755	0.103	0.469	0.812

Fig. 7 shows the Bode diagram of samples after 1, 72 and 168 h immersion in 3.5% NaCl. And Fig. 8 present corresponding SEM image of samples surface after 72 and 168 h immersion in 3.5% NaCl. Fig. 7a and b present the EIS of various coating after 1 h immersion. As observed in the phase angle plot (Fig. 7b), two time constants can be observed from the curve of samples after 1h immersion, one of which at high frequency corresponds to the sol-gel film response and another reflects the characteristic of low frequency which can be associated to capacitance of the electrochemical double layer on the substrate/electrolyte interface.

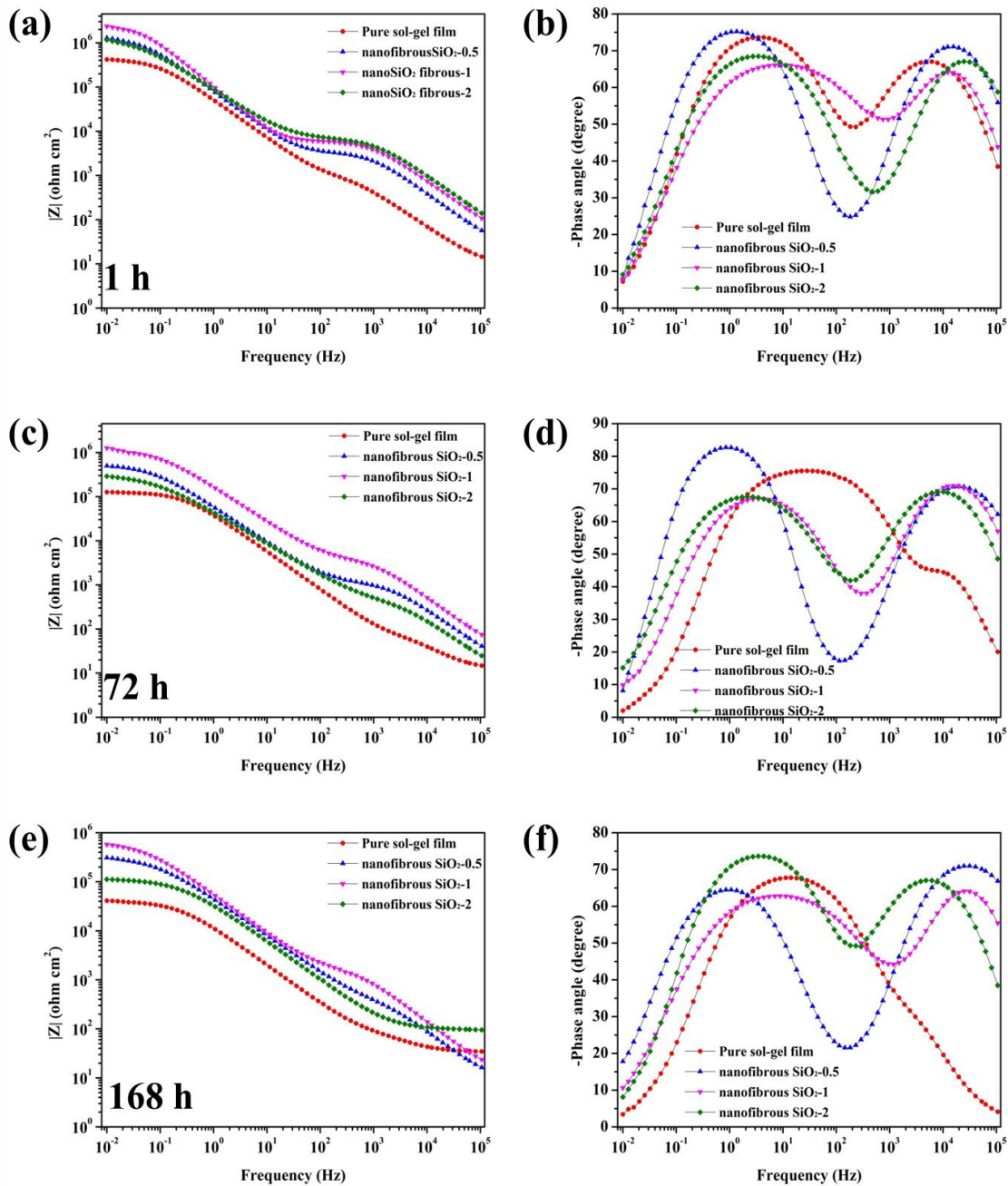


Figure 7. EIS curves and the fitting lines of pure sol-gel film and nanofibrous SiO_2 -0.5, nanofibrous SiO_2 -1 and nanofibrous SiO_2 -2 film coated AA5052 samples after 1, 72, 168 h in 3.5% NaCl solution. (a, b) after 1 h immersion; (c, d) after 72 h immersion; (e, f) after 168 h immersion.

The equivalent electric circuit (EEC) applied for numerical fitting of the EIS data is shown in Fig. 9. Two time constant equivalent electrical circuit was applied for sol-gel coated samples (as shown in Fig. 9a). The R_{sol} corresponds to the solution resistance. R_{coat} and Q_{coat} were assigned to the resistance and constant phase angle of the sol-gel coating.[31] The existence of ion-conducting paths in the sol-gel film can be evaluated.[32] The Q_{coat} can be associated with water uptake or entry of the

electrolyte into the coating.[33] R_{ct} and Q_{dl} correspond to charge transfer and the capacitance of the double layer in the electrolyte solution interface, the value of which also can reflect the substrate state. The derived parameters are presented in Table 2. Fig. 9b was applied for the sol-gel film coated sample without the time constant related the SiO_2 -0 film for 168 h immersion. Meanwhile, the evolution of $|Z|_{0.01Hz}$ value of sol-gel film coated samples also show in Fig. 10. The corrosion protection performance of the coating can be reflected from the low frequency impedance value, generally, a higher $|Z|_{0.01Hz}$ value in the modulus diagram suggests better corrosion protection performance of coating.[34]

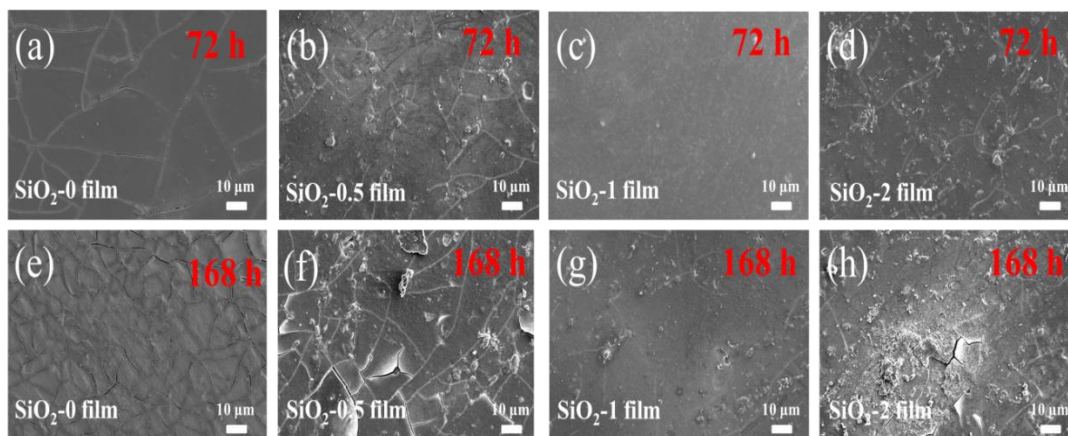


Figure 8. Surface morphology of sol-gel film modified by different amount nanofibrous SiO_2 at coated samples after 72 h and 168 h immersion in 3.5% NaCl aqueous solution

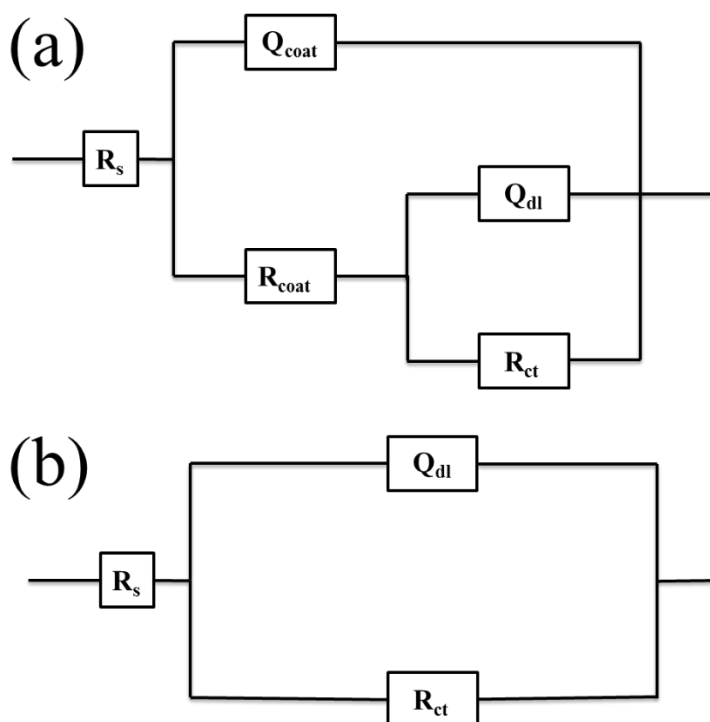
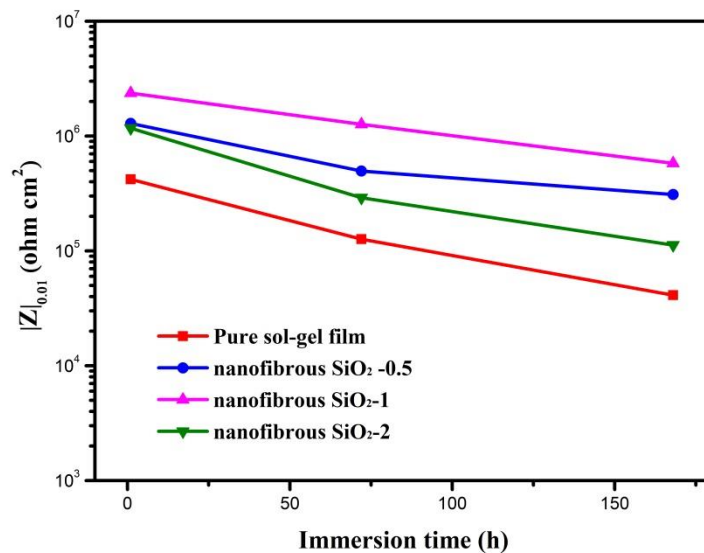


Figure 9. Electrochemical equivalent circuits used to fit the EIS data

Table 2. Resistances (R_{coat} , R_{ct}) and capacitance (Q_{coat} , C_{dl}) parameters extracted from EIS data within the test period

Coating	time (h)	Q_{coat}		R_{coat} ($\Omega \cdot \text{cm}^2$)	C_{dl}		R_{ct} ($10^5 \Omega \cdot \text{cm}^2$)	Chi-squared (10^{-3})
		$Y_0(\mu\text{S} \cdot \text{s}^n \text{cm}^{-2})$	n		$Y_0(\mu\text{S} \cdot \text{s}^n \text{cm}^{-2})$	n		
Sol-gel/nanofibrous SiO ₂ -0	1	2.37	0.84	1423	2.52	0.88	4.26	3.12
	72	3.31	0.80	128	2.80	0.85	1.36	4.12
	168	/	/	/	6.12	0.73	0.47	2.56
Sol-gel/nanofibrous SiO ₂ -0.5	1	0.137	0.89	3456	2.25	0.90	12.6	0.82
	72	0.237	0.88	1205	3.52	0.81	5.26	1.93
	168	0.737	0.86	500	4.53	0.74	3.26	3.14
Sol-gel/nanofibrous SiO ₂ -1	1	0.087	0.87	6205	1.54	0.98	22.6	0.74
	72	0.103	0.89	4205	1.22	0.81	11.6	0.47
	168	0.513	0.86	2014	3.13	0.79	6.16	3.14
Sol-gel/nanofibrous SiO ₂ -2	1	0.071	0.82	7103	3.34	0.89	11.6	2.24
	72	0.403	0.85	500	5.51	0.72	3.16	5.15
	168	1.031	0.50	100	5.73	0.80	1.16	1.97

**Figure 10.** The $|Z|_{0.01\text{Hz}}$ value of sol-gel film coated samples after immersion 1h,24h and 72h

It is observed that the $|Z|_{0.01\text{Hz}}$ value increase firstly with increasing nanofibrous SiO₂ concentration from 0 to 1 mg/mL (as shown in Fig. 10), the data suggest that the better barrier performance is achieved with addition of nanofibrous SiO₂, the SiO₂-1 film displayed the highly $|Z|_{0.01\text{Hz}}$ value. But the $|Z|_{0.01\text{Hz}}$ value show a reduction with concentration up to 2 mg/mL, which indicate that excess amount of nanofibrous SiO₂ led to decrease corrosion protection performance of sol-gel film. From the result, the evolution of R_{coat} and R_{ct} values with corresponding nanofibrous SiO₂ concentration show first increase and then decrease with increase in the concentrate of the nanofibrous SiO₂, and it is clear to obtain that the values of SiO₂-1 film shows highest value compare with the rest, which is consistent with the results obtained by SEM (as shown in Fig. 3d).

Fig. 7c and d show the Bode plots of different films after 72 h of immersion in 3.5% NaCl solution, $|Z|_{0.01\text{Hz}}$, R_{coat} and R_{ct} of all coating decrease with immersion time (as shown in Table 2 and Fig. 10). The $|Z|_{0.01\text{Hz}}$ value of the coating with 2 mg/mL concentrate decreases the most, followed by those with 0.5mg/mL and 1 mg/mL. The value of R_{coat} has the same pattern, which may duo to the

formation and growth of new cracks and pores[35]. The sharp drop in SiO₂-2 film is due to the many defects formation in the film caused by excess addition of nanofibrous SiO₂. Surface topography of SiO₂-1 coated sample still keeps intact and free from cracks (as shown in Fig. 8c). The micrographs of SiO₂-0 and SiO₂-0.5 film (Fig. 8a and b) show many cracks had formed on the surface of the coating, in constant, the SiO₂-2 coated sample formed more severely cracks (as shown in Fig. 8d).

The $|Z|_{0.01\text{Hz}}$, R_{coat} and R_{ct} values show a sustained decline for all coatings after 168 h immersion, while it decreases in varying degrees for coating with different concentration (as shown in Table 2 and Fig. 10). The disappearing coating response of SiO₂-0 film represents coating loose corrosion protection performance.[36] Simultaneously, the R_{coat} value of SiO₂-2 film drops to 100 Ω . The incorporation of nanofibrous SiO₂ at 1 mg/mL makes the film have significantly improved barrier properties and higher stability as confirmed from the R_{coat} and R_{ct} . After 168 h immersion, the surface topography of SiO₂-1 film appears film slight crack (as shown in Fig. 8g). More severe cracks appear on the surface of SiO₂-0.5 film and SiO₂-2 film (as shown in Fig. 8f and h), which led to a decrease in the corrosion protection performance of the sol-gel film.

The evolution of Q_{coat} values of the coating increases with immersion time. The coating capacitance can be associated with water uptake or entry of the electrolyte into the coating.[37] Q_{coat} values for the coating with nanofibrous SiO₂ are lower than the pure coatings, which also indicate improvement in protection behavior of the coating. However, a slight increase of Q_{coat} of SiO₂-1 film can be observed after long time immersion. In constant, the Q_{coat} of SiO₂-2 film increases rapidly. The corrosion protection performance of sol-gel film is reduced after long time immersion in the 3.5% NaCl solution.

4. CONCLUSIONS

The effect of addition concentration of nanofibrous SiO₂ on the structure, morphology, and corrosion protection performance of sol-gel film were investigated. The following conclusions were reached.

1. Among the four coatings, The SEM/TEM observations revealed that the nanofibrous SiO₂ additive disperses well in the sol-gel film. The addition of nanofibrous SiO₂ keeps the surface of the layer intact. The appropriate addition concentration of nanofibrous SiO₂ enhanced the cross-linking density of the sol-gel film and confirmed FTIR spectra.

2. In general, the influence of nanofibrous SiO₂ on the corrosion protection performance of the sol-gel film is positive: the current density decreases from 0.294 to 0.0581 $\mu\text{A}\cdot\text{cm}^{-2}$ when the additive concentration was increased from 0 to 1 mg/mL. However excess addition of nanofibrous SiO₂ caused the rapid increase in current. The results also confirmed from the EIS tests. The optimal concentration of nanofibrous SiO₂ is 1 mg/mL, at which concentration the coating resistance for the coating presented highest values. The higher corrosion protection performance of the coating can be ascribed to its compact microstructure. Meanwhile, there were no visible cracks formed on the surface of the film coated surface after 168h immersion in the 3.5% NaCl solution, which indicated excellent stability of the coating.

ACKNOWLEDGMENT

This work was supported by the financial support Shanghai Science and Technology (14DZ2261000)

References

1. J.H. Osborne, K.Y. Blohowiak, S.R. Taylor, C. Hunter, G. Bierwagon, B. Carlson, B. Dan, M.S. Donley, *Prog. Org. Coat.*, 41 (2001) 217. 1
2. M.A. Fardad, *J. Mater. Sci.*, 35 (2000) 1835.
3. L.L. Hench, J.K. West, *Chem. Rev.*, 90 (1990) 33.
4. W. Stöber, A. Fink, E. Bohn, *J. Colloid Interface Sci.*, 26 (1968) 62.
5. S. Amiri, A. Rahimi, *Iran. Polym.*, 25 (2016) 559.
6. A. Ershad-Langroudi, D. Zare, A. Rahimi, *Polym. Sci., Ser. A*, 59 (2017) 1.
7. M.F. Montemor, R. Pinto, G.S.M. Ferreira, *Electrochim. Acta*, 54 (2009) 5179.
8. H. Wang, R. Akid, *Corros. Sci.*, 49 (2007) 4491.
9. H. Wang, R. Akid, *Corros. Sci.*, 50 (2008) 1142.
10. R.Z. Zand, K. Verbeken, *Mater. Chem. Phys.*, 145 (2014) 450.
11. R. Supplit, T. Koch, U. Schubert, *Corros. Sci.*, 49 (2007) 3015..
12. J. Malzbender, J.M.J.D. Toonder, A.R. Balkenende, G.D. With, *Mater. Sci. Eng., R*, 36 (2002) 47.
13. Z.M. Shi, G.J. Ji, *Surf. Coat. Technol.*, 202 (2008) 1350.
14. S. Ono, H. Tsuge, Y. Nishi, S.I. Hirano, *J. Sol-Gel Sci. Technol.*, 29 (2004) 147.
15. G.M.S.E. Shafei, C.A. Philip, Z.A. Omran, *J. Therm. Anal. Calorim.*, 48 (1997) 373.
16. M. Yu, Y. Liu, J. Liu, S. Li, B. Xue, Y. Zhang, X. Yin, *Chin. J. Aeronaut.*, 28 (2015) 600.
17. S.A.S. Dias, S.V. Lamaka, T.C. Diamantino, M.G.S. Ferreira, *J. Electrochem. Soc.*, 161 (2014) C215.
18. L. Liu, J.M. Hu, J.Q. Zhang, C.N. Cao, *Electrochim. Acta*, 52 (2006) 538.
19. F. Yu, R. Akid, *Prog. Org. Coat.*, 102 (2017) 120.
20. B. Xue, M. Yu, J. Liu, J. Liu, S. Li, L. Xiong, *J. Alloys Compd.*, 725 (2017) 84.
21. A. Covelo, J. Genescá, A. Barba, C. Menchaca, J. Uruchurtu, M. Hernández, *Solid State Phenom.*, 227 (2015) 119.
22. M. Fedel, E. Callone, S. Diré, F. Deflorian, M.G. Olivier, M. Poelman, *Electrochim. Acta*, 124 (2014) 90.
23. L. Cheng, X. Ren, X. Wei, X. Sun, S. Yu, *Ser. Sci. Technol.*, 50 (2015) 700.
24. Y. Yamashita, M. Kaziwara, *J. Inorg. Organomet. P.*, 2 (1992) 129.
25. F. Babonneau, K. Thorne, J.D. Mackenzie, *J. Inorg. Organomet. P.*, 1 (1989) 26.
26. H. Habazaki, T. Kimura, Y. Aoki, E. Tsuji, T. Yano, *J. Electrochem. Soc.*, 161 (2014) C57.
27. S. John, A. Joseph, *Rsc Adv.*, 2 (2012) 9944.
28. S. John, A. Joseph, A.J. Jose, B. Narayana, *Prog. Org. Coat.*, 84 (2015) 28.
29. T. Kuila, S. Bose, C.E. Hong, M.E. Uddin, P. Khanra, N.H. Kim, J.H. Lee, *Carbon*, 49 (2011) 1033.
30. G.S. Frankel, *J. Test. Eval.*, 42 (2014) 517.
31. L. Vivar Mora, A. Taylor, S. Paul, R. Dawson, C. Wang, W. Taleb, J. Owen, A. Neville, R. Barker, *Surf. Coat. Technol.*, 342 (2018) 48.
32. M.L. Zheludkevich, R. Serra, M.F. Montemor, K.A. Yasakau, I.M.M. Salvado, M.G.S. Ferreira, *Electrochim. Acta*, 51 (2006) 208.
33. M. Schem, T. Schmidt, J. Gerwann, M. Wittmar, M. Veith, G.E. Thompson, I.S. Molchan, T. Hashimoto, P. Skeldon, A.R. Phani, S. Santucci, M.L. Zheludkevich, *Corros. Sci.*, 51 (2009) 2304.
34. A. Cabral, R.G. Duarte, M.F. Montemor, M.L. Zheludkevich, M.G.S. Ferreira, *Corros. Sci.*, 47 (2005) 869.
35. M.L. Zheludkevich, I.M. Salvado, M.G.S. Ferreira, *J. Mater. Chem. A*, 15 (2005) 5099.
36. M. Lu, J. Li, X. Yang, C. Zhang, J. Yang, H. Hu, X. Wang, *Chinese Sci. Bull.*, 58 (2013) 2698.

37. J. Liu, L. Hua, S. Li, M. Yu, *Appl. Surf. Sci.*, 327 (2015) 241.

© 2019 The Authors. Published by ESG (www.electrochemsci.org). This article is an open access article distributed under the terms and conditions of the Creative Commons Attribution license (<http://creativecommons.org/licenses/by/4.0/>).